Local Structure of a Rolled-Up Single Crystal: An X-Ray Microdiffraction Study of Individual Semiconductor Nanotubes

B. Krause, C. Mocuta, and T. H. Metzger
European Synchrotron Radiation Facility, Boîte Postale 220, F-38043 Grenoble Cedex, France

Ch. Deneke and O. G. Schmidt
Max-Planck-Institut für Festkörperforschung, Heisenbergstrasse 1, D-70569 Stuttgart, Germany
(Received 21 February 2006; published 27 April 2006)

Crystals with cylindrical symmetry, not existing in nature, are mimicked by the roll-up of single-crystalline and highly strained semiconductor bilayers. Exploiting this, the local structure of such individual rolled-up nanotubes is locally probed and quantified nondestructively by x-ray microbeam diffraction. A comparison to simulations, based on the minimization of the elastic energy, allows us to determine layer thicknesses and lattice parameter distributions within the strongly curved bilayers.

DOI: 10.1103/PhysRevLett.96.165502 PACS numbers: 61.10.Nz, 61.46.Fg

In recent years, great progress has been made in producing and integrating micro- and nanomechanical systems on a chip. Several approaches exist to create a vast variety of appropriate 3D objects, including lithographic methods and self-forming techniques. An intriguing combination of both approaches is the formation of rolled-up nanotubes (RUNTs) [1,2] which show great potential as integrative components such as 2D confined channels for fluid filling and transport [3], coils, transformers, capacitors [4], or optical wave guides [5]. To create a RUNT, a strained bilayer is partially released from a substrate by selective underetching. The free bilayer, still connected to the substrate on one side, relaxes the strain elastically by rolling up into a well-positioned microtube or nanotube. The tube radius is controlled by the layer thickness and the elastic properties of the bilayer [6]. This formation principle applies to many material systems, including semiconductors [1–7], hybrid materials [8,9], polymers [10], and metals [11].

RUNTs have a unique structure [12], since they consist of a crystalline layer which is oriented in all azimuthal directions. They nearly perfectly mimic a cylindrical symmetry which is not observed in natural crystals being described by translations of the crystal unit cell. While semiconductor RUNTs are in many ways similar to carbon nanotubes, their high crystalline quality and the wall thickness of several monolayers distinguishes them from other objects with cylindrical symmetry, such as, e.g., fibers and liquid crystals.

For understanding the formation process and the mechanical and electronic properties of the tubes, it is essential to measure their structure and final strain state. X-ray diffraction is a powerful tool to study strained semiconductor thin films in great detail [13]. Reducing the size of the x-ray beam by appropriate focussing optics, a high spatial resolution is obtained [14,15], allowing for the study of single micrometer-sized objects, in contrast to classical large-beam studies averaging over the diffraction of many micro-objects. The momentum transfer $\mathbf{q} = \mathbf{k}_f - \mathbf{k}_i$, where $\mathbf{k}_f$ and $\mathbf{k}_i$ are the wave vectors of the scattered and the incoming x-ray beam, is directly related to the lattice spacing d via $q = 2\pi/d$. Experimentally, the Bragg equation relates the momentum transfer to the scattering angle 2θ by $q = 4\pi \sin(2\theta/2)/\lambda$, where λ is the wavelength of the x rays. A lattice parameter distribution within a strained object can be studied by measuring the scattered x-ray intensity as a function of q, i.e., by changing the scattering angle.

Insight into the crystalline structure of RUNTs was previously gained by transmission electron microscopy [12,16–18] and micro-Raman spectroscopy [12,16]. TEM revealed that the rolled-up nanotubes can consist of radial superlattices with alternating crystalline and noncrystalline layers [12]. In Raman spectroscopy, vibration modes from the tube wall were consistent with shifts induced by the strain distribution [16]. However, both Raman spectroscopy and TEM require the separation of the RUNT from the substrate, thereby possibly influencing the tube structure. By TEM, the tube is studied in projection, whereas Raman scattering is only sensitive to the average structure probed by the finite-sized laser spot. Furthermore, it is not possible to study the crystalline interface within the bilayer.

In this Letter, we overcome such limitations and use nondestructive x-ray microbeam diffraction to study the local structure and, in particular, the lattice parameter distribution of GaAs/InGaAs RUNTs connected to the GaAs(001) substrate surface. Three different pseudomorphic GaAs/InGaAs bilayers [bilayers (I)–(III)], were grown on 4 nm AlAs sacrifical layers on GaAs(001) substrates. The thickness d_{Ga} of the GaAs layer was varied, whereas the thickness d_{In} and the In content $x = 0.215$ of the $\mathrm{In}_x\mathrm{Ga}_{1-x}\mathrm{As}$ layer were kept constant. In the as-grown film, the InGaAs layer is laterally compressed and vertically expanded.

The samples were scratched along the [100] direction and selectively underetched in a 3% HF solution. Starting from the scratches, the sacrifical layer was partially removed and the strained bilayer rolled up into microtubes and nanotubes. In the following, the tubes formed from the bilayers (I)–(III) are called RUNTs (I)–(III). Figure 1(a) shows a typical optical microscopy image of a sample after etching, where the scratches and the tubes can be identified. The tubes are situated between areas where the bilayer was removed from the substrate due to the rolling-up process, and areas still covered by the as-grown layers. Scanning electron microscopy (SEM) images of the studied tubes are shown in Fig. 2 (left). The tube radius R measured by SEM is given in Table I. R increases with increasing GaAs layer thickness. The rolled-up bilayers form multiwalled tubes with 5–6 rotations, aligned in the [100] direction of the substrate. The layer thickness (summarized in Table I) and composition of the as-grown bilayer were determined from x-ray reflectivity and diffraction measurements of the (004) Bragg reflection (not shown here). For all bilayers, the thickness of the natural oxide formed on the GaAs layer is about 1 nm, and the roughness of the layers is 0.2–0.3 nm.

The x-ray microbeam diffraction experiments were performed at the beamline ID01 of the European Synchrotron Radiation Facility (ESRF), at an energy $E = 10$ keV. The focussing of the x-ray beam to a spot size of 6×6 μm^2 at the sample position (intensity 1×10^9 photons/s, divergence about 20 mdeg) was accomplished using a circular Fresnel zone plate. For the measurements, a $4 + 2$ circle diffractometer with an avalanche photo diode as detector were used, integrating over the momentum transfer range $\delta q = 0.02$ Å^{-1} at the (004) peak of GaAs. The position of the sample was controlled by two orthogonally mounted optical microscopes. To prevent complete oxidation, the sample was kept in He atmosphere throughout the measurement.

A common approach in x-ray microbeam experiments is to localize the object with the help of its isotropically distributed fluorescence. Since the GaAs/InGaAs RUNTs are fixed to the GaAs substrate partially covered by the original GaAs/InGaAs bilayer, the substrate or bilayer fluorescence would render the identification of the tubes extremely difficult. Taking advantage of the fact that the RUNTs are well-aligned with respect to the substrate, it is nevertheless possible to align a specific position of a selected RUNT in the x-ray microbeam using a combination of optical alignment and diffraction.

First, the substrate is aligned in specular diffraction geometry. In this geometry, the incident angle α equals the scattering angle β, and the detector is positioned at 2θ [see Fig. 1(b)]. The selected tube is optically prealigned with the tube axis perpendicular to the incoming x-ray beam. Because of the rolling-up, the crystalline lattice of the tube is oriented isotropically perpendicular to the tube axis. The tube acts effectively as a 2D powder, and the isotropic scattering intensity in azimuthal direction is independent of α. By detuning the incident angle to $\alpha = \theta + \Delta$ [see Fig. 1(c)], the thermal diffuse background scattering of the substrate can be sufficiently reduced, so that the scattering of the RUNTs is discriminated from the

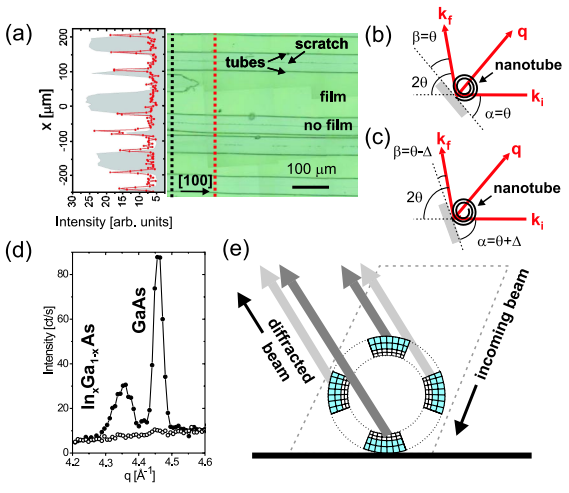

FIG. 1 (color online). (a) Correlation of an optical microscopy image with the x-ray measurements for determination of the tube position, (b) measurement geometry for specular diffraction, (c) measurement geometry after angular detuning, (d) radial scan of the (004) peak measured in detuned geometry on a tube (filled symbols) and on a laterally shifted position (open symbols), and (e) schematic of the scattering volume. For more details see text.

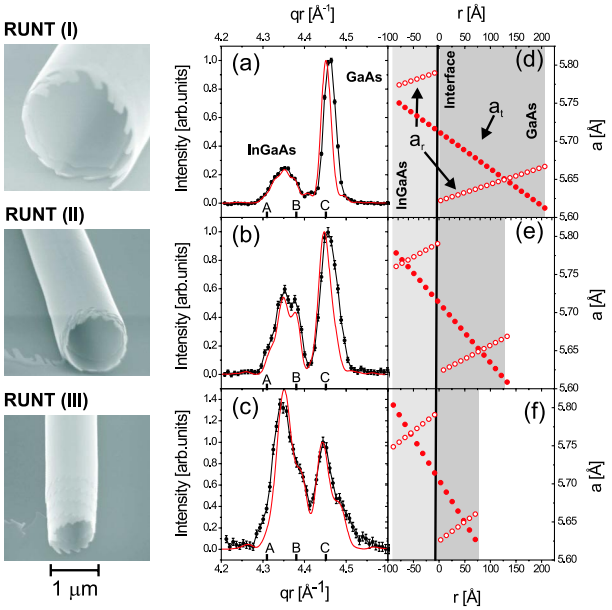

FIG. 2 (color online). Left: SEM images of RUNT (I)–(III). Center: Intensity distribution, normalized to the GaAs reflection, for (a) RUNT (I), (b) RUNT (II), and (c) RUNT (III). The experimental data are shown as black dots, the simulations as red lines. Right: lattice parameter distribution a_t in tangential direction (filled symbols) and a_r in radial direction (open symbols) as used for the simulations. For more details, see text.

TABLE I. Layer thickness of the as-grown bilayer, and values used for the simulation of the x-ray intensity distribution measured for the RUNTs shown in Fig. 2. The tube radius measured by SEM and resulting from the calculations (in brackets) are given.

Sample	d_{Ga} [nm]	d_{In} [nm]	R [μm]
bilayer (I)	22.4	9.4	
bilayer (II)	15.2	9.5	
bilayer (III)	9.1	9.5	
RUNT (I)	20.5	8.0	1.25 (1.18)
RUNT (II)	12.7	8.5	0.7 (0.73)
RUNT (III)	70.0	8.7	0.5 (0.52)

background signal. For identifying the exact position of the tube relative to the x-ray beam, two measurements are performed. (1) the sample is aligned in specular geometry on the (004) peak of the compressed InGaAs layer, and the scattering intensity is measured as a function of the sample translation in a direction perpendicular to the tube axis. (2) The incident angle is detuned by $\Delta \sim 15°$ and the scan is repeated at the estimated q of the (004) peak of the tube. An example of the alignment scans is shown in Fig. 1(a). The positions of the scan in specular geometry (dashed black line) and the scan in detuned geometry [dashed gray line (red online)] are indicated in the optical microscopy image. The measured intensity is shown at the left, on the same scale. The area with gray filling corresponds to the intensity measured in specular geometry. The intensity decreases at the positions where the film was removed. The dashed gray line (red online) indicates the position of a scan in detuned geometry. At the positions of the tubes, intensity maxima are observed [filled circles (red online)]. By correlating these measurements with the optical microscopy image, the position on the tube can be precisely identified with micrometer accuracy. Figure 1(d) shows the radial intensity distribution measured at a tube position (filled symbols) compared to the background intensity measured at a lateral position away from the tube (open symbols). The measurements were performed in detuned geometry, keeping the incident angle fixed and only changing the detector position. The signal of the tube shows two characteristic peaks and is clearly distinguishable from the monotonously increasing background signal.

Figure 2 compares the measured intensity distribution for RUNT (I)–(III) (black symbols). The intensity is normalized to the intensity of the GaAs reflection. For all measurements, two well-separated Bragg peaks are observed, one close to the bulk GaAs position marked as C and one between the strained InGaAs position A (found in the as-grown film perpendicular to the substrate) and the completely relaxed position B (i.e., the InGaAs lattice parameter expected from Vegard's law). The observation of two peaks shows that the crystalline bilayer is maintained in the RUNTs. As can be seen by the intermediate position of the InGaAs peak, the individual layers only partially relax because both of them exert a torsional moment on each other. With increasing GaAs layer thickness, the intensity ratio between the GaAs and the InGaAs peak increases. The shape of the peaks is determined by the interference of the x rays scattered by both layers.

The bending radius and the lattice parameter distribution of the RUNT were calculated by minimization of the total elastical energy, following Grundmann [19]. A tube with radius R and infinite length was assumed, formed by one turn of the bilayer with the thickness d_{In} of the InGaAs layer and the thickness d_{Ga} of the GaAs layer. Assuming isotropic elastical properties and planar stress, the elastical energy density ρ is

$$\rho = \frac{E}{2(1-\nu^2)}(\epsilon_t^2 + \epsilon_a^2 + 2\nu\epsilon_t\epsilon_a) \qquad (1)$$

where ϵ_t is the strain in tangential direction, ϵ_a the strain in direction of the tube axis, ν the Poisson ratio, and E the Young's modulus. The strain in radial direction is coupled to the strain in the other directions by $\epsilon_r = \frac{\nu}{\nu-1}(\epsilon_t + \epsilon_a)$. The strain along the tube axis is constant and independent of the distance r from the interface between the two layers. It can be written as $\epsilon_a = a_a/a - 1$ where a_a is the lattice constant along the tube axis and a is the unstrained lattice parameter. The tangential strain can be written as $\epsilon_t(r) = (a_t/a - 1) + a_t r/(aR)$ where a_t is the tangential lattice constant at the interface and r is the radial distance to the interface. The total strain energy $E_{tot}(a_t, a_a, R)$ is calculated by integrating Eq. (1) over the entire tube radius. E_{tot} is minimized as a function of its variables, and neglecting higher orders of $1/R$ the solution for the geometric tube shape and the lattice parameter distribution is determined analytically.

From the lattice parameter distribution, the x-ray intensity was calculated in kinematic approximation. Only lattice planes oriented perpendicular to the momentum transfer contribute to the measured intensity [schematically shown in Fig. 1(e)]. For the studied tubes, the scattering is dominated by the two sectors with the radial planes oriented perpendicular to the momentum transfer (indicated by dark arrows), while the sectors with the azimuthal lattice planes oriented perpendicular to $\mathbf{q}$ (light arrows) can be neglected. The contributions of the different sectors depend strongly on the bending of the tube, the divergence of the incoming beam, and the detector acceptance, as has been verified by simulations. The experiment gives a local structure information which is limited to a scattering volume much smaller than the illuminated part of the tube.

For the simulations presented in Figs. 2(a)–2(c) [gray line (red online)], it was assumed that the tube can only relax in tangential and radial direction, but not along its axis. The elasticity of the materials was described by the Young's modulus E and the Poisson ratio ν, using $E = 85.3$ GPa and $\nu = 0.312$ for GaAs, and extrapolating $E = 78.2$ GPa and $\nu = 0.321$ for InGaAs. The parameters used

for the simulations are summarized in Table I. The calculated lattice parameter distribution in radial and tangential direction is plotted as a function of r [Figs. 2(d)–2(f)]. For clarification, the region within the GaAs layer ($r > 0$) is underlaid in dark gray, the region within the InGaAs layer ($r < 0$) in light gray. Filled symbols correspond to the tangential lattice constant which is continuous as a function of r. The radial lattice constant (open symbols) is discontinuous at the interface, as a consequence of the different unit cell sizes and elastical properties of InGaAs and GaAs. In order to reproduce the experimentally measured x-ray intensity, for all tubes the crystalline layer thickness had to be reduced by about 1 nm for the InGaAs layer and about 2.5 nm for the GaAs. The effective roughness is within 0.2–0.5 nm similar to the roughness of the original film. As a consequence of small inhomogeneities of the tube, the scattering of several turns adds up incoherently. The measurements are therefore well reproduced with a model based on a single tube wall. The differences in the strain distribution of the subsequent turns can be neglected as well, as has been verified by simulations varying the inner tube radius.

Additional simulations were performed based on a slightly different model, allowing for a free relaxation along the tube axis. The best fit for RUNT (III), the tube with the lowest d_{Ga}, was found for the model without axial tube relaxation. For RUNT (I) and (II), both simulations agree well with the measured data. This result confirms the intuitive assumption that tubes with a radius much smaller than their length are hindered in their axial expansion if they are fixed to a substrate along their entire length. However, some relaxation along the axis might arise due to crack formation and dislocations.

The reduction of the crystalline layer thickness compared to the as-grown bilayer is related to a strongly disturbed crystalline structure at the bonding interface between subsequent turns originating from a misfit of about 2.1%. During the rolling-up, a small amount of the etching solution is included at the bonding interface. It is likely that the water reacts with the crystalline material, increasing the thickness of the disturbed layer by forming an amorphous oxide-rich layer of a thickness limited by the amount of water included. Amorphous oxide-rich layers at the bonding interface were observed in TEM measurements of similar tubes [12,17].

In summary: we have performed x-ray microbeam diffraction measurements of a series of single InGaAs/GaAs semiconductor nanotubes connected to the substrate. We exploit the cylindrical symmetry of the tubes to study the scattering of this extremely small amount of strained material. The measured intensity distribution is completely described using a model based only on the elastic relaxation of the bilayer, assuming that the tube relaxation along its axis is hindered by the connection with the substrate. We have shown that x-ray microbeam diffraction is a nondestructive probe to study the local structure of individual rolled-up nanotubes. Our technique promises to be useful for the study of rolled-up crystalline layers of various compositions, thicknesses, and sizes, thus helping to understand their fundamental functional properties in future integrated devices.

We acknowledge helpful discussions with R. Songmuang and N.-Y. Jin-Phillipp. C. D. and O. G. S. acknowledge financial support by the BMBF (03N8711).

[1] V. Y. Prinz, V. A. Seleznev, A. K. Gutakovsky, A. V. Chekhovskiy, V. V. Preobrazhenskii, M. A. Puyato, and T. A. Gavrilova, Physica (Amsterdam) **6E**, 828 (2000).
[2] O. G. Schmidt and K. Eberl, Nature (London) **410**, 168 (2001).
[3] C. Deneke and O. G. Schmidt, Appl. Phys. Lett. **85**, 2914 (2004).
[4] O. G. Schmidt, C. Deneke, S. Kiravittaya, R. Songmuang, H. Heidemeyer, Y. Nakamura, R. Zapf-Gottwick, C. Müller, and N. Y. Jin-Phillipp, IEEE J. Sel. Top. Quantum Electron. **8**, 1025 (2002).
[5] S. Mendach, R. Songmuang, S. Kiravittaya, A. Rastelli, M. Benjoucef, and O. G. Schmidt, Appl. Phys. Lett. **88**, 111120 (2006).
[6] C. Deneke, C. Müller, N.-Y. Jin-Phillipp, and O. G. Schmidt, Semicond. Sci. Technol. **17**, 1278 (2002).
[7] M. H. Huang, C. Boone, M. Roberts, D. E. Savage, M. G. Lagally, N. Shaji, H. Qin, R. Blick, J. A. Nairn, and F. Liu, Adv. Mater. **17**, 2860 (2005).
[8] O. G. Schmidt, N. Schmarje, C. Deneke, C. Müller, and N. Y. Jin-Phillipp, Adv. Mater. **13**, 756 (2001).
[9] O. Schumacher, S. Mendach, H. Welsch, A. Schramm, C. Heyn, and W. Hansen, Appl. Phys. Lett. **86**, 143109 (2005).
[10] V. Luchnikov, O. Sydorenko, and M. Stamm, Adv. Mater. **17**, 1177 (2005).
[11] Y. V. Nastaushev, V. Y. Prinz, and S. N. Svitasheva, Nanotechnology **16**, 908 (2005).
[12] C. Deneke, N.-Y. Jin-Phillipp, I. Loa, and O. G. Schmidt, Appl. Phys. Lett. **84**, 4475 (2004).
[13] U. Pietsch, V. Holý, and T. Baumbach, *High-Resolution X-Ray Scattering from Thin Films and Lateral Nanostructures* (Springer-Verlag, Berlin Heidelberg, 2004).
[14] J. D. Budai, W. Yang, N. Tamura, J.-S. Chung, J. Z. Tischler, B. C. Larson, G. E. Ice, C. Park, and C. P. Norton, Nat. Mater. **2**, 487 (2003).
[15] D. Loidl, O. Paris, M. Burghammer, C. Riekel, and H. Peterlik, Phys. Rev. Lett. **95**, 225501 (2005).
[16] R. Songmuang, N.-Y. Jin-Phillipp, S. Mendach, and O. G. Schmidt, Appl. Phys. Lett. **88**, 021913 (2006).
[17] N.-Y. Jin-Phillipp, J. Thomas, M. Kelsch, C. Deneke, R. Songmuang, and O. G. Schmidt, Appl. Phys. Lett. **88**, 033113 (2006).
[18] V. Y. Prinz, A. V. Chekhovskiy, V. V. Preobrazhenskii, B. R. Semyagin, and A. K. Gutakovsky, Nanotechnology **13**, 231 (2002).
[19] M. Grundmann, Appl. Phys. Lett. **83**, 2444 (2003).